Available online at www.sciencedirect.com
SCIENCE DIRECT®
Journal of Hydrology 322 (2006) 220–235
Journal of Hydrology
www.elsevier.com/locate/jhydrol

Scaling analysis of space–time infiltration based on the universal multifractal model

H. Meng[a], J.D. Salas[a,*], T.R. Green[a,b], L.R. Ahuja[a,b]

[a]Department of Civil Engineering, Colorado State University, Fort Collins, CO 80523, USA
[b]Great Plains Systems Research Unit, USDA-ARS, Fort Collins, Co 80526, USA

Abstract

There is broad interest in the space–time scaling behavior of infiltration over a watershed, but field data is lacking to identify such scaling and the controlling factors. Here, theoretical effects of rainfall and saturated hydraulic conductivity (K_s) on space–time infiltration are simulated using process-based numerical experiments in the framework of a universal multifractal (UM) model. A series of rainfall and K_s fields are generated including both random, non-scaling fields and multifractal fields produced using the UM model. By varying the UM model parameters based on physical considerations, rain and K_s fields with various scaling characteristics are obtained. These rain and K_s data are then fed into a distributed rainfall-runoff model developed for this study to produce space–time infiltration, including the effects of overland flow from upslope areas. The scaling properties of the infiltration are then analyzed to find the impact from the rain and K_s fields mainly in terms of the connections among the UM model parameters between the input and the output fields. Some of the major findings from this research are: (1) rainfall spatial characteristics determine the scaling of infiltration only at very early times; (2) K_s, rather than rain, determines if the resulting infiltration field displays scaling behavior after an adjusting period; (3) generally, the heterogeneity of a rain field and the singularity and sparseness of a K_s field have strong impacts on infiltration; (4) usually, infiltration fields are statistically non-homogeneous; and (5) if an infiltration field subject to space–time rain becomes less singular (localized large infiltration rates) in time, it tends to become less sparse and more heterogeneous, and vice versa. The relationships and sensitivities identified above help us understand some key factors controlling the potential scaling behavior of infiltration.

Keywords: Infiltration; Rainfall-runoff; Soil water; Process simulation; Scaling; Multifractal

1. Introduction

Surface infiltration is a vital component of the hydrologic cycle; its importance has been realized for many years and numerous studies have been devoted to the subject (e.g. Maller and Sharma, 1981; Dagan and Bresler, 1983; Revol et al., 1997; Govindaraju et al., 2001). Previous research on infiltration has contributed primarily to our understanding of point infiltration processes. However, surface infiltration is characterized by considerable spatial and temporal variations. Efforts to incorporate such variability in point infiltration parameters based on the so-called equivalent homogeneous parameters may not be valid

* Corresponding author. Tel.: +1 970 491 6057; fax: +1 970 491 7727.
E-mail address: jsalas@engr.colostate.edu (J.D. Salas).

0022-1694/$ - see front matter © 2005 Elsevier B.V. All rights reserved.
doi:10.1016/j.jhydrol.2005.03.016

in general. For example, Bresler and Dagan (1983, p. 425) concluded "…stochastic modeling has to be employed in order to derive the averaged variables and the concept of equivalent uniform soil is not valid." To improve the accuracy of estimating infiltration, there is a need for improved understanding of the complex temporal and spatial features of infiltration, including effects of run-off/run-on between land areas. Surface infiltration is closely related to the characteristics of the driving forces such as rainfall and saturated hydraulic conductivity (K_s). The connection between the temporal and spatial variability of such driving forces with infiltration is another topic that has not received enough attention in the literature.

Various approaches have been employed in the literature to represent the temporal and spatial variability of infiltration. Among them, Maller and Sharma (1981) assumed lognormal distributions for the parameters in the Philip's infiltration model and determined the corresponding distribution of infiltration flux. Dagan and Bresler (1983) used Green and Ampt's (1911) moving front concept and the assumption of effective parameters to derive the expectation and variance of the water flux as functions of depth and time. Sivapalan and Wood (1986) derived the cumulative distribution of ponding time from lognormally distributed saturated hydraulic conductivity (K_s) by using derived distribution theory, and then obtained some quasi-analytical expressions for estimating the mean and variance of infiltration as functions of rainfall and K_s statistics. More recently, Govindaraju et al. (2001) provided expressions for describing the ensemble-averaged field-scale infiltration and predicting the time it took for a given areal depth of water to infiltrate into the soil. These expressions were derived assuming that saturated hydraulic conductivity is represented by a homogeneous correlated lognormal random field, and infiltration followed the Green–Ampt model, but the effects of run-off/run-on were not considered.

Olsson (2002) analyzed the spatial variability of soil–water redistribution in field soils based on digitized images of dye 24 h after infiltration from experiments carried out on three sites. Their research showed that infiltration/redistribution in field soils displayed multiscaling characteristics. They also fitted the universal multifractal (UM) model to the dye infiltration data and found that the simulated fields reproduced key features of the observed data. To our knowledge, the work of Olsson et al. has been the only infiltration research conducted in the framework of scaling. As described above, the majority of the previous work done on the spatial variability of infiltration has been based on traditional statistical or stochastic approaches. The outcomes of the studies are usually expressed as the general statistics of the infiltration fields that are only suitable to the scale at which the studies were conducted. Scaling theory is an excellent approach for dealing with stochastic processes across scales, provided the processes are scaling. Some of the main driving forces of the infiltration process, such as rainfall, hydraulic conductivity, and topography, have been found to display scaling behavior (Lovejoy and Schertzer, 1990; Over and Gupta, 1994; Tessier et al., 1996; Liu and Molz, 1997; Lavallée et al., 1993). Moreover, some related processes that influence infiltration, such as soil moisture, have also been shown to display scaling behavior (e.g. Rodriguez-Iturbe et al., 1995; Peters-Lidard et al., 2001; Green and Erskine, 2004). Considering the close connection between surface infiltration and these scaling fields, it is logical to hypothesize the scaling nature of infiltration.

The objective of this study is to acquire a better understanding of the spatial and temporal variability of surface infiltration processes. Specifically, this objective is achieved by exploring the effects of two of the main driving force and soil parameter, namely rainfall and saturated hydraulic conductivity (K_s), on infiltration using numerical experiments. A series of rainfall and K_s fields are generated including both random non-scaling fields and multifractal fields. By varying the model parameters, rain and K_s fields with various characteristics are obtained. These rain and K_s data are then fed into a rainfall-runoff model to produce the resulting infiltration field. The spatial and temporal variability of infiltration are then examined using scaling analysis to discern the effects from the rain and K_s fields. Section 2 introduces the methods employed in this study, such as the UM model used to generate rainfall and K_s fields, and the rainfall-runoff model utilized for determining the infiltration field. Section 3 describes the general set-up of the numerical experiments performed, such as the study area, topography of the site, and the choices of the various

model parameters. The specific results of the numerical experiments are presented in Section 4 where the infiltration fields resulting from two types of rainfall fields—steady and space–time—are examined. Finally, Section 5 is dedicated to the summary and conclusions of this research.

2. Methods

The study of the spatial and temporal variability of infiltration, which is described herein, is based on simulated rainfall and saturated hydraulic conductivity fields that are applied to a small watershed in eastern Colorado. Although the watershed has topographic data and soil characteristics, no spatial rainfall nor run-off data are available at that location. Thus, the experimental study described herein is based on simulated rainfall using parameters that have been determined elsewhere and using a rainfall-runoff model that has been calibrated and validated using a USDA-ARS experimental watershed. The saturated hydraulic conductivity K_s has been generated based on soil properties measured at the referred watershed. Despite the sparseness of available data, the study has used procedures, models, and parameters that have been widely discussed and published in literature.

The overall method followed in the research reported herein may be summarized in three major steps, namely: (1) simulation of the rainfall field based on a multifractal model, (2) simulation of the corresponding infiltration field by means of a topographically-based distributed rainfall-runoff model, and (3) scaling analysis and modeling of the simulated infiltration field. The rainfall field was simulated based on the UM model developed by Schertzer and Lovejoy (1987) and based on a lognormal random field. A rainfall-runoff model (Meng, 2004) was used to determine the infiltration field. The model was developed using well-known physical–mathematical relationships representing the various components of the hydrologic cycle of the watershed. The infiltration component of the model is a function of K_s. To account for the spatial variability of K_s, UM and lognormal random field models were utilized. Finally, the simulated infiltration field was analyzed and fitted using a UM model to verify the degree to which the field possesses multifractal scaling properties. To explain the method in some detail we first describe in Section 2.1 below some underlying concepts of the UM model along with parameter estimation and goodness of fit criteria for the UM model. In addition, we include in the Appendix A a summary of the algorithm for generating a UM field. The rainfall-runoff model is briefly described in Section 2.2, summarizing its basic features, but a full description of the model can be found in Meng (2004). Then, Section 2.3 discusses the procedure followed for analyzing the scaling characteristics of the simulated infiltration field.

2.1. Universal multifractal model

The most fundamental characteristic of a scaling system is its scale invariance, i.e. its small and large-scale statistical properties are related by a scale-changing operation involving only the scale ratio (Tessier et al., 1993). Two types of scaling processes have been observed in the physical world: simple scaling and multiscaling. In the language of fractals, a simple scaling field is defined by one fractal set and corresponds to a single fractal dimension, i.e. a simple scaling field is monofractal. A multiscaling field consists of a series of random scale functions rather than a single function (as in the case of simple scaling.) Each of these scale functions is defined by a fractal subset, which often has a unique fractal dimension or codimension (Schertzer and Lovejoy, 1987). Therefore, a multiscaling field is also called a multifractal field (Parisi and Frisch, 1985). Simple scaling is often too restrictive to hold for complex geophysical processes. Multiscaling is a more general framework for scale-invariant non-linear dynamics. For convenience the term ‘scaling’ is used throughout when referring to a multiscale system.

The model used for generating scaling rainfall and K_s fields is the UM model developed by Schertzer and Lovejoy (1987). This model also sets the framework for the scaling analysis performed on surface infiltration herein. A brief summary of the generating algorithm based on the UM model is given in Appendix A. More complete descriptions of the UM model can be found in, e.g. Schertzer and Lovejoy (1987) and Pecknold et al. (1993). The UM model has the advantage of fully characterizing a multifractal field with only three parameters: α, C_1 and H, where α is the

Lévy index; C_1 is the codimension of the mean process; and H is the non-conservation parameter. The Lévy index characterizes the degree of multifractality of a scaling field (as opposed to monofractal). Large α corresponds to a significant singularity in the field. The codimension C_1 defines the sparseness of the average level of the field. The non-conservation parameter H indicates the deviation of the observed field from the underlying conservative (or statistically homogeneous) field. Thus, $H=0$ corresponds to a conservative (or statistically homogeneous) field while a large H represents a high degree of heterogeneity in the scaling field (Lavallée et al., 1993). By systematically varying the three parameters within their respective ranges, which are predefined based on physical considerations, rainfall and hydraulic conductivity fields with various characteristics can be obtained.

The double trace moment (DTM) technique is used to estimate the UM model parameters (α and C_1) from conservative fields (Lavallée et al., 1993). The initial estimate of the parameter H of a non-conservative field may be obtained from the qth-order structure function (Schmitt et al., 1995; Liu and Molz, 1997):

$$E[|R(z+h)-R(z)|^q] = E[(\Delta R_h)^q] = Ah^{\xi(q)} \tag{1}$$

where R is a multifractal function, $E[\,]$ denotes expected value; z is distance; h is distance increment or lag; q is the order of structure function; and A is a function of q. It may be shown that for $q=1$ (i.e. first-order structure function) $\xi(q)=H$. Thus, an initial estimate of H may be obtained from the slope of the log–log plot of the first-order structure function versus the distance increment. A fractional differentiation of order initial H is applied to the non-conservative field to achieve the *initial* underlying conservative field. The parameters α and C_1 of this initial conservative field are then estimated using the DTM technique. Meng (2004) found that the estimate of α is very sensitive to the estimate of H if the conservative field is obtained through fractional differentiation. Thus, she suggested a refined estimation procedure that can produce the more accurate estimates of the UM model parameters. In the subject of this paper we followed the DTM technique with the refinement suggested by Meng (2004).

To evaluate the goodness of fit of the UM model that is fitted to a certain field we compare the β estimated from the power spectrum of the (sample) field and the 'theoretical' value obtained from the equation (Lavallée et al., 1993)

$$\beta = 2H - \frac{C_1(2^\alpha - 2)}{\alpha - 1} + 1 \tag{2}$$

For spatial processes that evolve through time (such as the infiltration process that we study herein) one could make the comparison for a specific time or for a range of times. In our study, when applying this goodness-of-fit approach to the space–time infiltration processes, we determine the relative root mean square difference between the estimated $\hat{\beta}$ and the 'theoretical' β in 10-min increments (rather than the comparison of the β values at single points in time). This value, denoted as RRMSD_β_I, measures how close the estimated and theoretical βs are. Denoting the estimated β at 10-min intervals as $\hat{\beta}$, and the corresponding 'theoretical' β, RRMSD_β_I is defined as

$$\mathrm{RRMSD\_}\beta_I = \sqrt{\frac{1}{n}\sum_{i=1}^{n}\left(\frac{\hat{\beta}_i - \beta_i}{\beta_i}\right)^2} \tag{3}$$

where n is the number of 10-min intervals considered in the simulation experiment.

2.2. Rainfall-runoff model

A physically based, distributed rainfall-runoff model was developed for the study on surface infiltration (Meng, 2004). This model employs the D-infinity flow direction model (Tarboton, 1997) to define the routing hierarchy of a watershed down to pixels. The D-infinity model is also used to delineate the watershed for calibration and validation, and to determine channels within the watershed. The event-based rainfall-runoff model can handle variable rainfall both in space and in time. Ponding time is computed using a model that also can handle variable rainfall. Hortonian run-off is taken to be the mechanism for run-off generation, which is consistent with observations. The Green–Ampt model is used to compute infiltration capacity. Both run-off and run-on are taken into consideration in the calculation of infiltration. A kinematic wave model is adopted for both overland and channel flow routing. Numerical approximations to the routing equations employ an

implicit finite difference scheme. Since the channels in the study area (Section 3.1) are ephemeral, no base flow has been considered in the rainfall-runoff model.

The rainfall-runoff model was calibrated and validated using rainfall and run-off data collected from the sub-watershed 11 (WG11) of the USDA-ARS Walnut Gulch experimental watershed located in a semi-arid area in Arizona. A sensitivity analysis identified porosity and K_s as the most significant parameters in their influence on the run-off of WG11. Hence the pair of parameters was taken as the calibration parameters. Different categories were identified throughout WG11 for each calibration parameter based on measurements and/or watershed conditions. The relative magnitudes of the categories were kept fixed during calibration and a uniform multiplier was applied to each calibration parameter. Five rainfall-runoff events were used for calibration and gave satisfactory results. The pair of parameters chosen from calibration was then applied to nine rainfall-runoff events to validate the rainfall-runoff model. The validation results showed that the model could reasonably replicate the distributed watershed processes such as infiltration and run-off over a watershed—making it an acceptable rainfall-runoff model for the scaling studies that follow (for more details, cf. Meng, 2004).

2.3. Scaling criteria

Before any scaling analysis can be performed on a given field, the field must be shown to have scaling behavior. A few approaches have been reported in the literature to assess the scaling behavior of a given field by exploring the moments, structure function, and power spectrum, etc. (e.g. Gupta and Waymire, 1990; Tessier et al., 1993; Schmitt et al., 1995; Liu and Molz, 1997). The power spectrum method is chosen in this study for checking whether a field is scaling (all physical fields are assumed to be isotropic in this research). The power spectrum of a scaling field has the following form:

$$E(k) \approx k^{-\beta} \tag{4}$$

where $E(k)$ is power spectrum, k is wavenumber, and β is a constant greater than zero. Eq. (4) suggests that the power spectrum of a scaling field is log–log linear against wavenumber with a negative slope. Radial power spectrum is used in this research because the fields of our study (e.g. infiltration) are embedded in a 2D space. A radial power spectrum is obtained by angular integration in Fourier space.

Since the log-linearity of power spectra is an indication of scaling, one must use a metric to check whether the sample spectrum of a given field is log–log linear; a modified R^2 or coefficient of determination is used. The conventional R^2 suffers from an angle dependency. Therefore, the power spectrum of a physical field is first rotated to $\omega = -1$, where ω is the slope of the linear regression line after rotation, before its R^2 is calculated. This approach is similar to using a Nash and Sutcliffe (1970) measure of model efficiency, where the predicted values come from the idealized scaling model (Eq. (4)). Fig. 1 shows the power spectrum of a scaling field, its R^2 value (0.0576) and the spectrum after angle rotation with its modified R^2 value (0.9898). Experiments were conducted in order to determine a criterion based on the value of the modified R^2 (called mR^2 hereafter for the modified coefficient of determination). The average mR^2 obtained from 108 generated multifractal fields is 0.945 (Meng, 2004). Because of the uncertainties involved in simulating the infiltration process, a more relaxed reference value of 0.90 is taken herein to assess the linearity of the power spectrum of the infiltration fields. Meng (2004) showed that such a reduction in the reference value is necessary to account for a reasonable amount of noise (i.e. uncertainty) in the output fields. It is noted that the reference mR^2 value is intended to be an

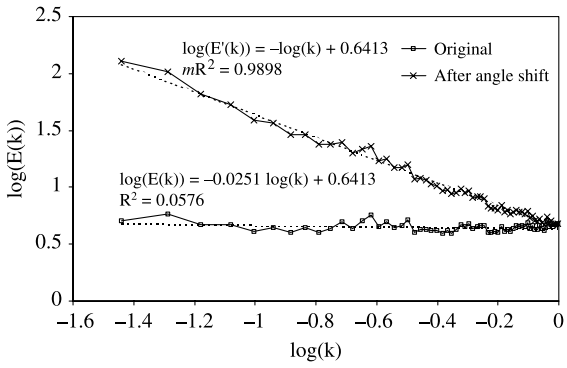

Fig. 1. Power spectrum of a scaling field with $R^2 = 0.0576$ and the modified spectrum after angle rotation with modified $R^2 = 0.9898$.

indicator of scaling behavior rather than a cutoff value for scaling field. It would be physically unrealistic to impose such a strict cutoff value. Thus, two terms are used in this study to describe a field as 'strongly scaling' or 'scaling' depending on whether its mR^2 is above or below 0.945, but fields with mR^2 values smaller than 0.9 are judged to be non-scaling. In addition to the required mR^2 value, the original regression angle needs to be negative for a scaling field to ensure that large features of a field contribute more to the power spectrum than small features ($\beta > 0$ in Eq. (4)).

3. Description of the experiments

The general approach of this numerical study is to generate both scaling and non-scaling rain and K_s fields, input these simulated driving fields to the rainfall-runoff model (Section 2.2) applied to a real topography and soil properties, derive the resulting space–time surface infiltration fields, and analyze the statistical and scaling properties of the infiltration fields such as the field average infiltration rate, mR^2 of logarithm of power spectrum, and fit and evaluate the UM model to the infiltration field at 10-min intervals.

3.1. Study area

A USDA-ARS experimental site on the Lindstrom Farm near Sterling, Colorado, USA is chosen to be the study area for the numerical experiments. This is a semi-arid area with high-intensity summer thunderstorms. It has some ephemeral streams where Hortonian overland flow is the predominant mechanism for run-off generation. The DEM data of the area has been obtained from the USGS, and has a 30-m resolution with 128×128 pixels. Thus, the size of the study area is about 14.7 km^2. The channels of the area are defined using a contributing area threshold. The defined channels compare favorably with the results of a county survey. The dominant soil type of the study area is loam. Fig. 2 shows the channels in the study area.

3.2. Model parameters

Both conservative and non-conservative rain fields have been observed in nature (Tessier et al., 1993; Pecknold et al., 1993; Harris et al., 1996). Tessier et al. (1993) reported that the scaling parameters for radar rain fields are $\alpha = 1.35$, $C_1 = 0.3$, and $H = 0$ (i.e. homogeneous); and the parameters from raingauge data are $\alpha = 1.35$, $C_1 = 0.2$, and $H = 0$. Based on this information, the rain rate model parameters are chosen to be in the ranges $\alpha = 1.2$–1.8, $C_1 = 0.2$–0.4, and $H = 0$–0.5, where non-zero H values are used to simulate non-conservative (non-homogeneous) rain fields. Some random lognormal rain fields were also used in this study. Fig. 3 shows examples of generated scaling rain fields based on the UM model with parameters $\alpha = 1.5$, $C_1 = 0.3$, and $H = 0$, 0.1, 0.2, and 0.5.

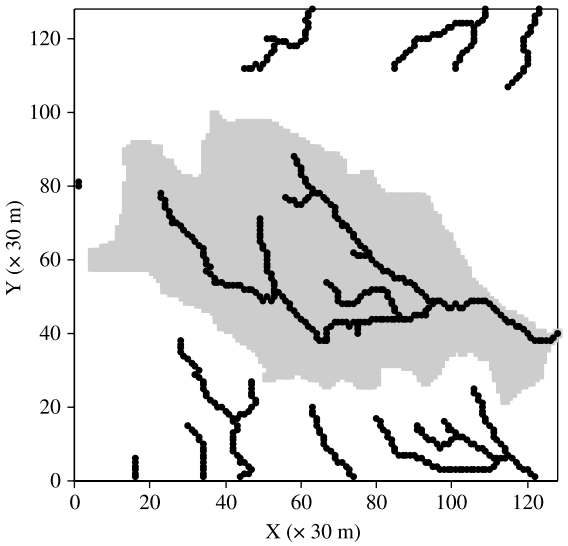

Fig. 2. Defined channels in the small watershed at the ARS experimental site on the Lindstrom Farm near Sterling, Colorado.

Some studies report that K_s and $\ln(K_s)$ data are multifractal in horizontal and/or vertical directions (Liu and Molz, 1997; Tennekoon et al., 2003). Also 144 steady state infiltration measurements collected for the R-5 catchment at Oklahoma (Loague and Gander, 1990) and additional data of hydraulic conductivity taken at 15 locations in the R-5 catchment (Ahuja et al., 1984) have been analyzed and shown to be scaling. In our study, the horizontal K_s field is assumed to be multifractal and conforms to the UM framework. The following parameter ranges are used in the numerical experiments: $\alpha = 1.5$–2.0, $C_1 = 0.01$–0.05, and $H = 0$–0.5 where $\alpha = 2.0$ corresponds to the lognormal multifractal case. The small

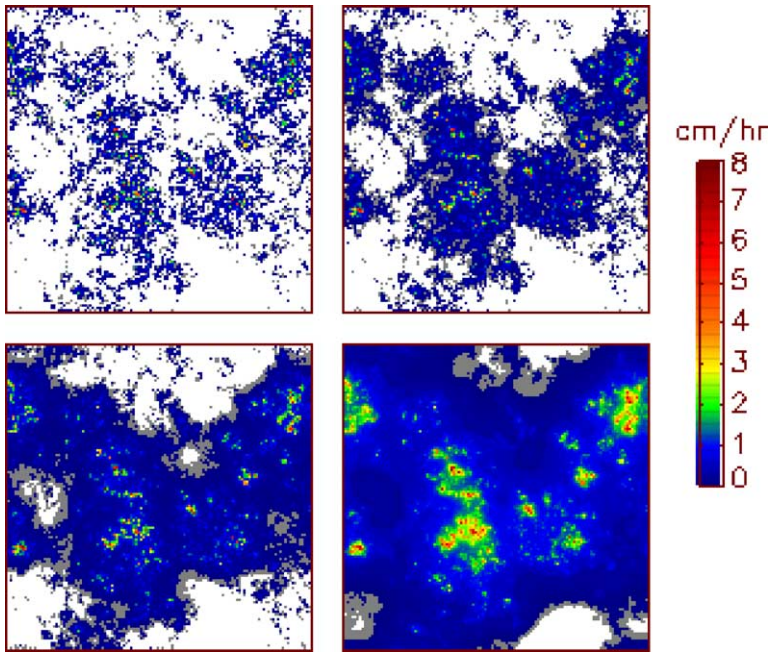

Fig. 3. Rain fields generated by a UM model with parameters (a) $\alpha_R=1.5$, $C_{1R}=0.3$, and $H_R=0.0$; (b) $\alpha_R=1.5$, $C_{1R}=0.3$, and $H_R=0.1$; (c) $\alpha_R=1.5$, $C_{1R}=0.3$, and $H_R=0.2$; and (d) $\alpha_R=1.5$, $C_{1R}=0.3$, and $H_R=0.5$.

C_1 values are used because natural K_s fields are known to have little sparseness. Random lognormal K_s fields were also applied in some cases. Fig. 4 shows three examples of generated scaling K_s field based on the UM model with parameters $C_1=0.01$, $H=0.2$, and $\alpha=1.5$, 1.75, and 2.0.

The porosity of loam (value of porosity of loan used here) is applied throughout the study area in the rainfall-runoff model. The field capacity, residual soil moisture content, and wetting front suction at overland pixels are assumed to be functions of K_s and are derived from K_s through empirical equations while

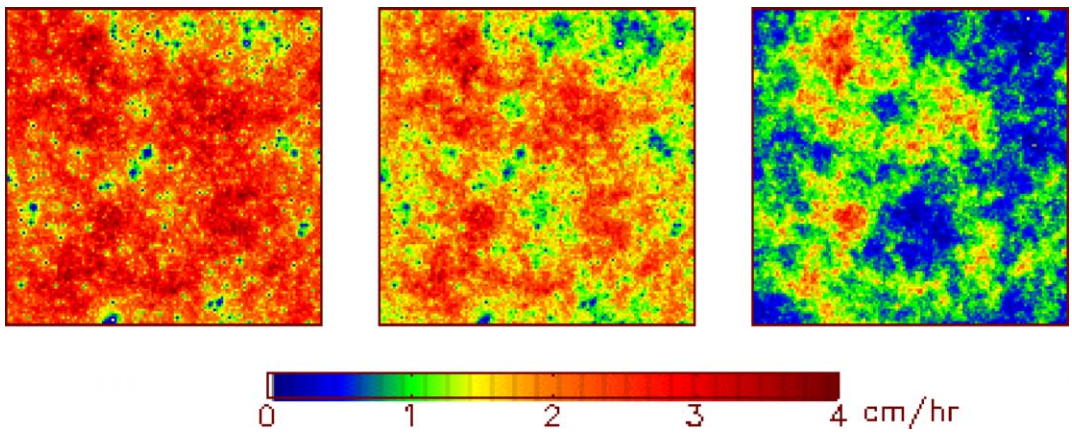

Fig. 4. K_s fields generated by a UM model with parameters (a) $\alpha_{K_s}=1.5$, $C_{1K_s}=0.01$, $H_{K_s}=0.2$; (b) $\alpha_{K_s}=1.75$, $C_{1K_s}=0.01$, $H_{K_s}=0.2$; and (c) $\alpha_{K_s}=2.0$, $C_{1K_s}=0.01$, $H_{K_s}=0.2$.

they are constants at channel pixels with typical values for loam soil. Manning's n for overland flow with a field crop is used for hillslope pixels; and Manning's n for natural, clean, basically straight channels is used for channel pixels. Considering the semi-arid nature of the study area, the initial soil moisture is set to be dry in channels and medium dry elsewhere throughout this study.

For each of the cases examined in the following study, 25 simulations are run and the average quantities are analyzed for scaling behavior. This quasi-Monte Carlo approach is used to minimize the uncertainty caused by the randomness of the generated input fields.

4. Results

The first group of rainfall-runoff experiments is performed under the assumption of steady rainfall, that is, the rain rate field is variable in space but constant through time. Both scaling and non-scaling steady rain and K_s fields are tested for their effects on infiltration processes. The influence of scaling space–time rainfall and scaling K_s fields on infiltration is also examined with a series of experiments. The following notations are used for subscripts below: R represents rain rate, K_s represents K_s, and I represents infiltration.

4.1. Non-scaling steady rain and scaling K_s

Twenty-five lognormally distributed random rain fields are generated with a mean of 3 cm/h and a standard deviation of 3 cm/h. The rain fields are characterized by white noise and have an average radial power spectrum with $\beta_R = -1.02$ (Fig. 5). A scaling K_s field is generated using the UM model with a mean of 1.32 cm/h and the following scaling parameters: $\alpha_{K_s} = 2.0$, $C_{1K_s} = 0.01$, and $H_{K_s} = 0.2$. Its power spectrum has a $\beta_{K_s} = 1.32$ and $mR^2_{K_s} = 0.97$ (Fig. 5). Therefore, the K_s field is a strongly scaling field. Each of the 25 steady rain fields and the scaling K_s field are input to the rainfall-runoff model to derive the corresponding space–time infiltration processes. Fig. 5 shows the offset average power spectrum of the infiltration fields at several points in time, along with the average power spectrum of the steady rain fields and the power spectrum of the K_s field. It is observed that the power spectrum of the infiltration field resembles that of the steady rain field at the beginning of the infiltration process, and as time evolves it gradually becomes more similar to that of the K_s field especially at lower wavenumbers. This observation is in agreement with the known fact that rainfall has a dominant effect on surface infiltration in the early stage of an infiltration process, and soil properties (particularly K_s) become more important than rain in determining the properties of the infiltration field as rainfall continues. The slopes and the values of mR^2_I of the average infiltration power spectra are plotted in Fig. 6 (note the dual Y-axes). This figure reveals that the infiltration field is non-scaling in the early stage of the process as indicated by the positive slope of the power spectrum. As time progresses, the slope turns negative and the mR^2_I becomes stable at a level around the mR^2 reference value, suggesting that the infiltration field

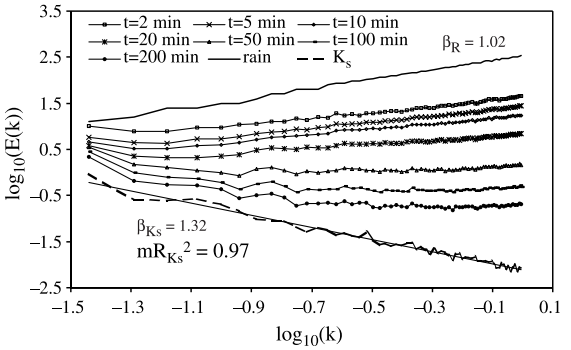

Fig. 5. Average power spectrums of infiltration fields under non-scaling steady rainfall and scaling K_s field (the lines have been offset for clarity).

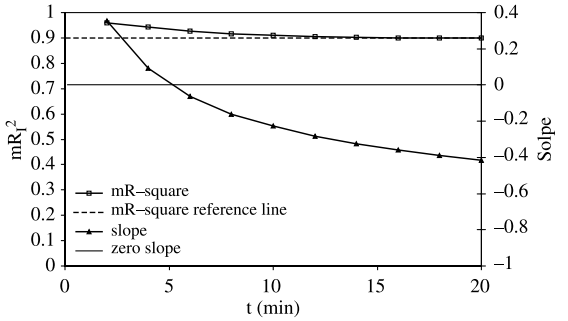

Fig. 6. Slopes and mR^2_I of the average power spectrums of infiltration fields under non-scaling steady rainfall and scaling K_s field.

becomes scaling. It is concluded from this set of experiments that a non-scaling rain field determines the non-scaling nature of its corresponding infiltration field in the early stage of the process. However, such an infiltration field eventually becomes scaling where the K_s field is scaling.

4.2. Scaling steady rain and non-scaling K_s

To test the effect of scaling steady rain and non-scaling K_s on infiltration, 25 lognormally distributed random K_s fields are generated with a mean of 1.32 cm/h and a standard deviation of 0.7 cm/h. The average power spectrum of the K_s fields has $\beta = -1$ (Fig. 7), i.e. the K_s fields are characterized as white noise. The scaling rain field used in these experiments is generated using the UM model. It has a mean of 3 cm/h and the following parameters: $\alpha_R = 1.5$, $C_{1R} = 0.2$, and $H_R = 0.5$. Its power spectrum has a $\beta_R = 1.59$ with $mR_R^2 = 0.97$ (Fig. 7), which reveals that the rain field is strongly scaling.

Fig. 7 shows the power spectra of the corresponding infiltration fields at a few points in time along with the power spectra of the rain and K_s fields. The power spectra of the infiltration fields show a dominant effect from the rain field at the early stage and a gradually stronger influence from the K_s field as time progresses especially at the high wavenumbers. The time series of the slopes and the mR_I^2 of the average power spectra are presented in Fig. 8. It shows that the infiltration field is scaling for a short period of time at the beginning of the infiltration process because of the influence of the scaling rain, and then becomes non-scaling as revealed by the small mR_I^2 value (about 0.76) and the rapidly increasing spectrum slope. These results demonstrate that an infiltration process will be scaling at the early stage if the rain field is scaling, but will become non-scaling in time as long as the K_s field is non-scaling.

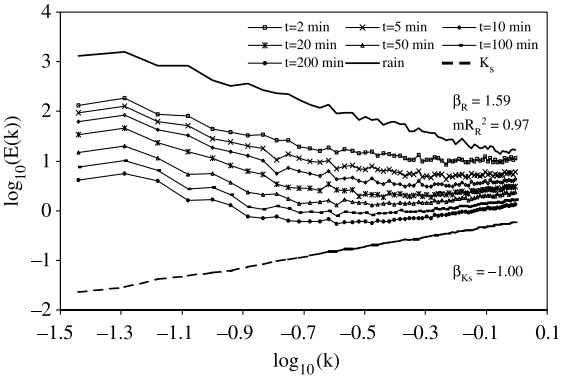

Fig. 7. Average power spectrums of infiltration fields under scaling steady rainfall and non-scaling K_s field (the lines have been offset for clarity).

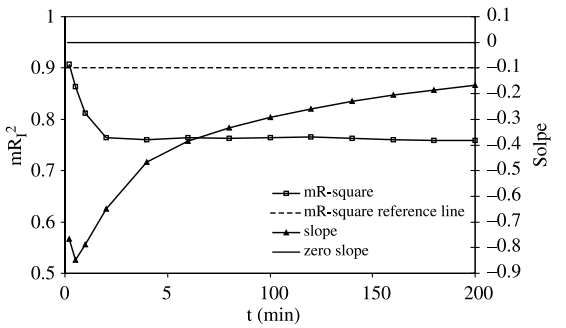

Fig. 8. Slopes and mR_I^2 of the average power spectrums of infiltration fields under scaling steady rainfall and non-scaling K_s field.

4.3. Scaling steady rain and scaling K_s

Three UM model parameters of both the scaling steady rain fields and the scaling K_s fields are examined for their respective effect on infiltration. The rain parameter α_R is the first one to be analyzed through three sets of experiments. Each set has the same C_{1R} (0.2) and H_R (0.2) but different α_R (1.2, 1.5,

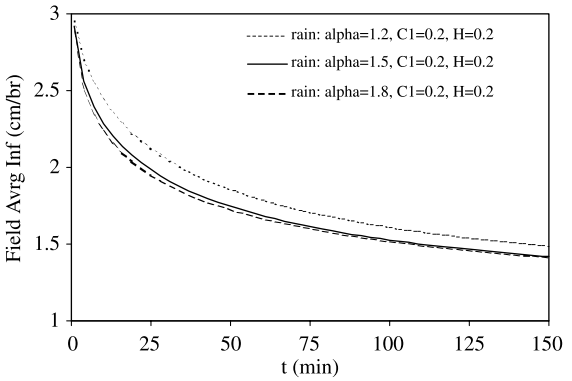

Fig. 9. Effect of α_R on the field average surface infiltration rates under scaling steady rain fields and scaling K_s field ($\alpha_{K_s} = 2.0$, $C_{1K_s} = 0.01$, and $H_{K_s} = 0.2$).

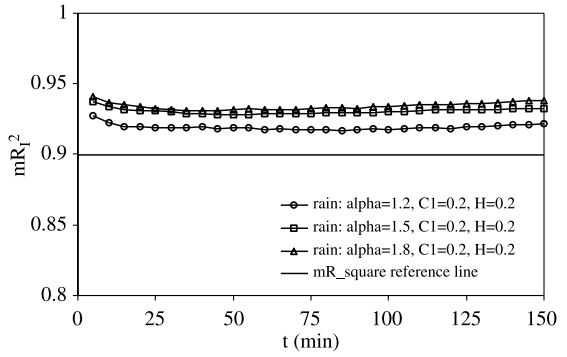

Fig. 10. Effect of α_R on mR_I^2 of the infiltration fields under scaling steady rain and scaling K_s fields ($\alpha_{K_s}=2.0$, $C_{1K_s}=0.01$, and $H_{K_s}=0.2$).

or 1.8). The scaling K_s field used in all the experiments is generated using the UM model with the following parameters: $\alpha_{K_s}=2.0$, $C_{1K_s}=0.01$, and $H_{K_s}=0.2$. Fig. 9 shows the field average infiltration rates for the three sets of rain fields. It is observed that the field average infiltration increases as α_R becomes smaller.

Combined with the scaling K_s field, all three scaling rain fields yield scaling infiltration fields for all times, as the high values of the mR_I^2 of the power spectra in Fig. 10 indicate good log-linearity of the power spectra. It is noted that the power spectra of infiltration fields always have negative slopes under scaling rain and scaling K_s.

Fig. 11 compares the 'theoretical' and the estimated β of the infiltration fields from the first set of rain. The RRMSD_β_I of the estimated β series is 0.08—indicating that the UM model fits to the infiltration process well. In this case, the estimated β appears to converge to the 'theoretical' β—indicating that the UM model fits better to the infiltration field as the latter develops. It is important to point out that a large degree of uncertainty is involved in determining the value of RMSD_β_I. Besides the fact that the 'theoretical' β is essentially an estimate itself, the estimated β is also very sensitive to the range of wavenumbers used to

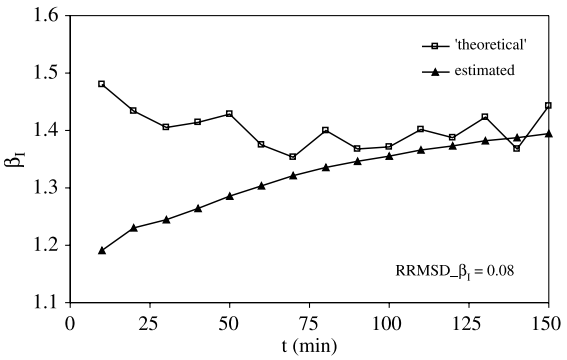

Fig. 11. Comparison of the theoretical and the estimated β_I of the infiltration field under scaling steady rain field ($\alpha_R=1.2$, $C_{1R}=0.2$, $H_R=0.2$) and scaling K_s field ($\alpha_{K_s}=2.0$, $C_{1K_s}=0.01$, and $H_{K_s}=0.2$).

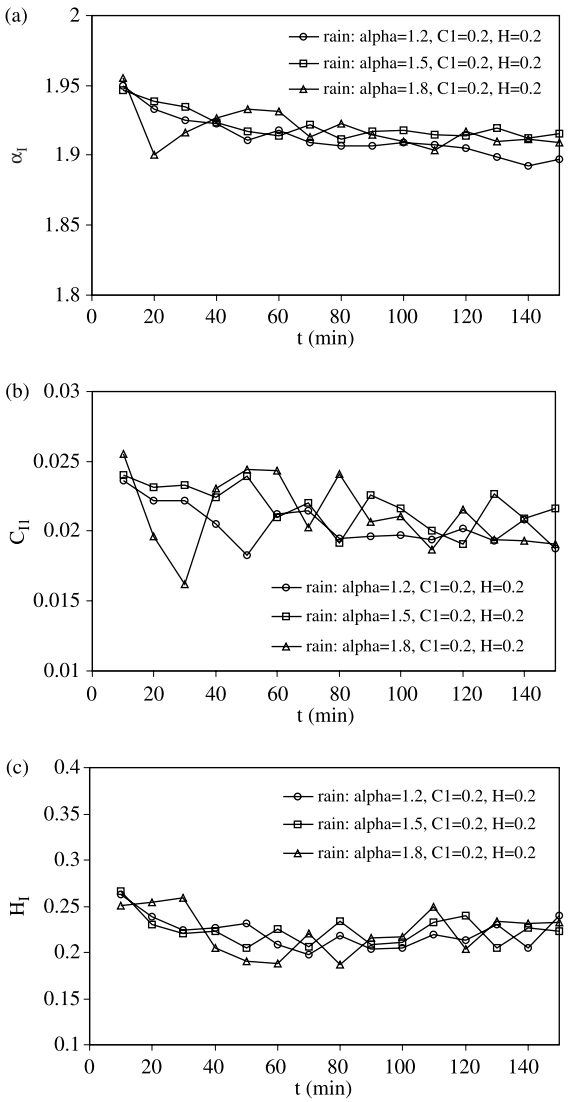

Fig. 12. Effect of α_R on the estimated infiltration parameters (a) α_I, (b) C_{1I}, and (c) H_I, under scaling steady rain fields and scaling K_s field ($\alpha_{K_s}=2.0$, $C_{1K_s}=0.01$, and $H_{K_s}=0.2$).

derive the parameter. The power spectrum corresponding to the 10 lowest wavenumbers are used in this study to estimate β. Fig. 12 presents the time series of the estimated infiltration scaling parameters from the three sets of experiments. Little systematic variation is observed in the infiltration parameters as α_R changes. Therefore, it is concluded that the singularity of the rain field has minor effect on the scaling properties of the infiltration field.

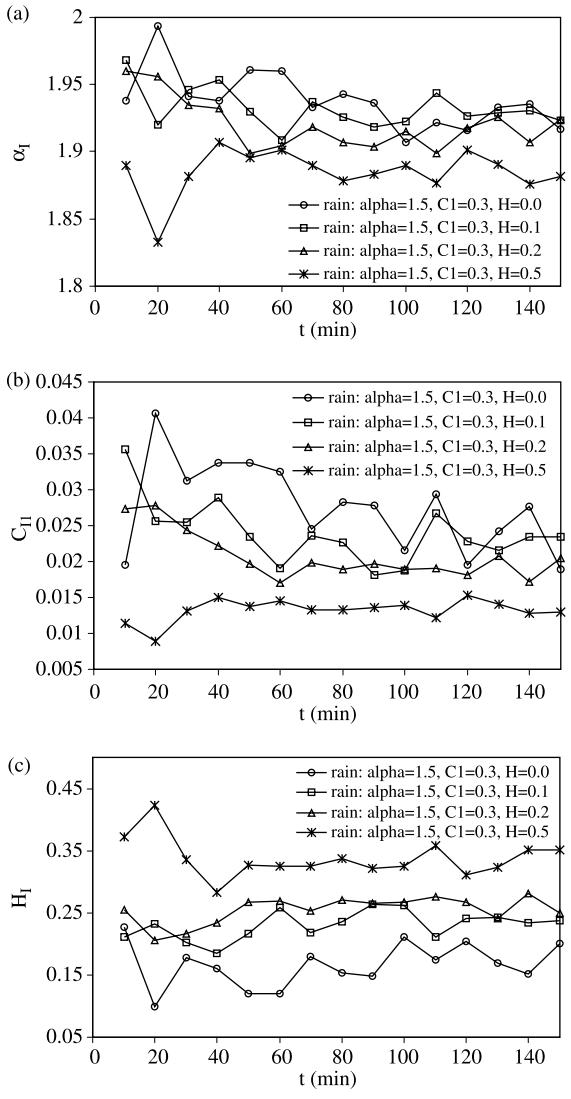

Fig. 13. Effect of H_R on the estimated infiltration parameters (a) α_I, (b) C_{1I}, and (c) H_I, under scaling steady rain fields and scaling K_s field ($\alpha_{K_s}=2.0$, $C_{1K_s}=0.01$, and $H_{K_s}=0.2$).

To examine the effect of rain parameter H_R on infiltration, four sets of rain fields are generated, each with different H_R (0.0, 0.1, 0.2, or 0.5) but the same α_R (1.5) and C_{1R} (0.3). The K_s field employed has the following parameters: $\alpha_{K_s}=2.0$, $C_{1K_s}=0.01$, and $H_{K_s}=0.2$. The corresponding infiltration fields are found to be either strongly scaling or scaling. Fig. 13 shows the time series of the estimated infiltration parameters. The influence of the rain heterogeneity (H_R) on infiltration is strong. Rain heterogeneity is proportional to infiltration heterogeneity and inversely proportional to the singularity and sparseness of infiltration field.

Table 1 summarizes the effects of rainfall and K_s parameters on the various aspects of infiltration fields as observed in the numerical experiments performed above. Only the most significant influences are specified by up or down arrows (indicating positive or negative correlation between the input field parameters and the infiltration properties). It is noted that the singularity of a K_s field only shows a strong effect on the singularity and sparseness of an infiltration field when the former approaches 2.0, i.e. α_{K_s} is large.

4.4. Scaling space–time rain and scaling K_s

Rainfall in the real world is characterized by variations both in space and in time. Thus, it is essential to add the temporal dynamics of rain field to the study of infiltration process. In the absence of a practical space–time rain model that fits into the framework of UM, a series of 'space–time' rain fields is generated using the UM model as explained below.

First, a large rain field with 2048×2048 pixels—the largest scaling field that can be generated with the available computer resources—is generated using the UM model. Then consecutive cutouts from this large field with the size of 128×128 pixels are taken as 'space–time' rain fields at one pixel apart. This in effect adds advection to a steady rain field. If advection is assumed to be 10 m/s, moving one pixel at a time translates to a time step of 3 s, and a total of 96 min of rainfall can be extracted from the large rain field. Ninety-minute 'space–time' rainfalls are applied to the experiments carried out in this section. The average rain intensity of the large rain field is 3 cm/h.

To examine the effect of H_R on infiltration, four types of rain fields are generated with the following

Table 1
Effect of parameters of scaling steady rain and scaling K_s on infiltration

	Average field infiltration rate (cm/h)	Scaling (minimum mR_I^2)	Average RRMSD_β_I	Singularity (α_I)	Sparseness (C_{1I})	Heterogeneity (H_I)
α_R	–	Yes (0.92)	0.09	–	–	–
C_{1R}	↓*	Yes (0.92)	0.10	–	–	–
H_R	↑	Yes (0.89)	0.19	↓	↓	↑
α_{K_s}	–	Yes (0.90)	0.06	($\alpha_{K_s} \longrightarrow^{\uparrow} 2.0$)	($\alpha_{K_s} \longrightarrow^{\uparrow} 2.0$)	–
C_{1K_s}	–	Yes (0.91)	0.07	–	–	–
H_{K_s}	–	Yes (0.89)	0.05	–	–	–

*↑ means strong positive correlation, ↓ means strong negative correlation, and – means weak to medium correlation. mR_I^2 is the modified coefficient of determination for infiltration scaling.

parameters: $\alpha_R = 1.2$, $C_{1R} = 0.2$, and $H_R = 0.0$, 0.1, 0.3, or 0.5. At the early stage of the infiltration process, when the soil is fairly dry, the field average infiltration rate of the resulting infiltration fields is negatively correlated to H_R (Fig. 14). This correlation becomes small and even reverses direction as soil becomes more saturated in time. The dynamics introduced in the space–time rain are responsible for the different pattern in the field average infiltration from the simple case of steady rain.

The infiltration fields under the four sets of rain fields are scaling (minimum $mR_I^2 = 0.88$). Fig. 15 displays the time series of the estimated scaling parameters of the infiltration fields. The rain heterogeneity shows a strong and non-unidirectional influence on the infiltration parameters. The singularity and the sparseness of the infiltration fields are proportional to the rain heterogeneity if the rain field is homogeneous ($H_R = 0$) or close to homogeneous, but become inversely proportional to the latter as the rain field becomes more heterogeneous. The heterogeneity of the infiltration fields varies with the rain in the opposite direction to the singularity and sparseness of the infiltration fields. Other important features of the infiltration process under the space–time rain are the temporal trends exhibited in the time series of the scaling parameters. While these trends are somewhat detectable in some of the steady rain cases, they are consistent and more clear in all of the experiments under the space–time rain. It is observed that the directions of the temporal trends are determined by the rain heterogeneity. The singularity (α_I) and the sparseness (C_{1I}) of the infiltration field decrease in time if the rain field has a low degree of heteogeneity. Otherwise, the two parameters will reverse the trend and increase in time. The heterogeneity of the infiltration field has a rising temporal trend if the rain field is more homogeneous, but does not show a clear trend as the rain field becomes highly heterogeneous.

All the scaling parameters of the space–time rain and K_s fields are investigated for their individual effects on infiltration. Table 2 summarizes the results from these experiments. Arrows are used to mark only the strongest correlations between rain and K_s parameters and infiltration properties. Some differences are evident between these infiltration fields and those under steady rain, although they share many common features. In particular, we see the dominant effects of H_R on all of the scaling parameters of the resulting infiltration fields.

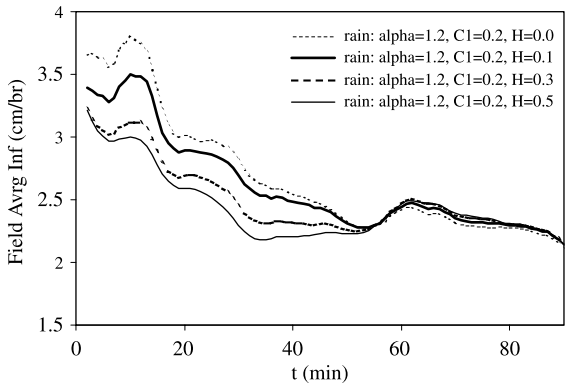

Fig. 14. Effect of H_R on the field average surface infiltration rates under scaling space–time rain fields and scaling K_s field ($\alpha_{K_s} = 2.0$, $C_{1K_s} = 0.01$, and $H_{K_s} = 0.2$).

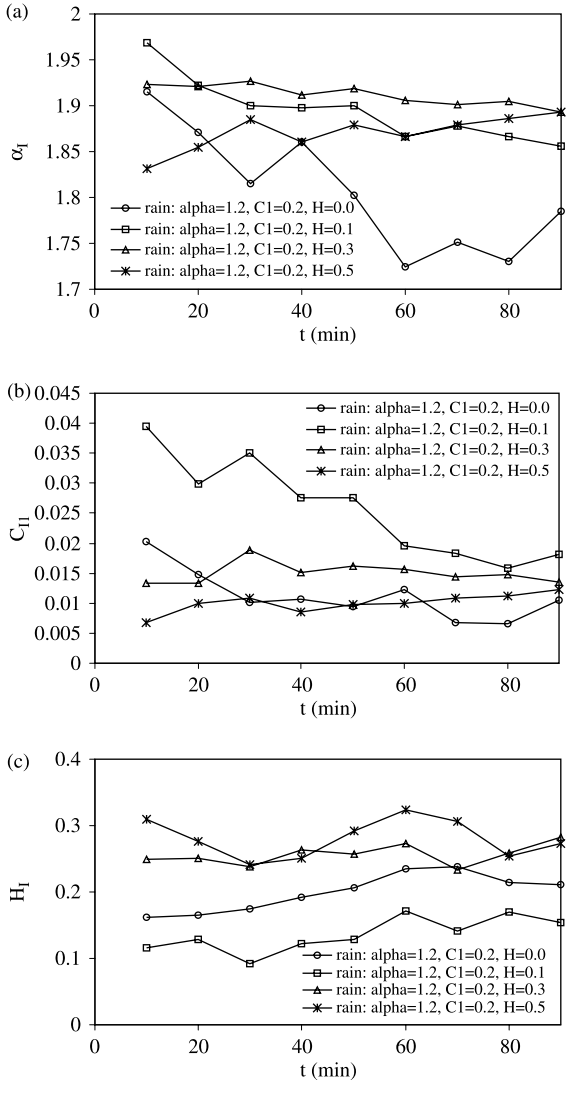

Fig. 15. Effect of H_R on the estimated infiltration parameters (a) α_I, (b) C_{1I}, and (c) H_I, under scaling space–time rain fields and scaling K_s field ($\alpha_{K_s}=2.0$, $C_{1K_s}=0.01$, and $H_{K_s}=0.2$).

5. Summary and conclusions

Rainfall and K_s fields with various characteristics have been generated and used as input to a Hortonian rainfall-runoff model to produce space–time infiltration processes. The properties of the infiltration processes, such as the traditional statistics, power spectrum, and scaling characteristics are then analyzed to find the impacts on scaling behaviors of the infiltration fields. Some criteria are defined in this research to assess the scaling behavior of the infiltration fields and to judge the goodness of fit of the UM model to the infiltration fields. The UM model parameters of the infiltration fields are then estimated using a refined approach developed for estimating UM model parameters of non-conservative scaling fields.

Non-scaling steady rainfall and hydraulic conductivity fields are first tested for their general influences on infiltration. If the rain field is non-scaling, but the K_s field is scaling, the infiltration process is found to become scaling eventually. The infiltration field will become non-scaling soon after rain stops. On the other hand, if the K_s field is non-scaling, the infiltration process will be non-scaling, except at very early times, if the rainfall field is scaling. Hence, the K_s field rather than the rain field determines if the resulting infiltration field is scaling after an adjusting period.

A series of steady (i.e. constant in time) scaling rainfall and scaling K_s fields are generated using the UM model to study their effects on infiltration. The corresponding infiltration fields are either strongly scaling or scaling throughout the processes. The UM model can be fitted to the majority of the infiltration fields with a high degree of agreement. The estimated UM model parameters show that the sparseness and the stastical heterogeneity of the rain field have the strongest effects on the watershed-average infiltration rate. Less sparse and more heterogeneous rain will lead to more infiltration on average. This result would not be expected without simulating the processes of run-on and subsequent augmented infiltration at downslope positions, which demonstrates the importance of including such process-based spatial interactions in our model. The heterogeneity of a steady rain field has the strongest effect on infiltration among the scaling parameters of the rain field. More heterogeneous rain fields usually lead to more heterogeneous, less singular, and more space-filling infiltration fields. However, the homogeneous rain fields employed in this study did not produce homogeneous infiltration fields. Strong singularity in K_s fields also plays an important role in determining the scaling properties of infiltration. More singular K_s fields correspond to more singular and sparser infiltration fields. The homogeneous K_s fields also did not yield homogeneous infiltration fields in this study.

Table 2
Effect of parameters of scaling space–time rain and scaling K_s on infiltration

	Average field infiltration rate (cm/h)	Scaling (minimum m R_I^2)	Aerage RRMSD_β_I	Singularity (α_I)	Sparseness (C_{1I})	Heterogeneity (H_I)
α_R	↓*	Yes (0.91)	0.12	–	–	–
C_{1R}	–	Yes (0.91)	0.07	–	–	–
H_R	(dry soil↓)	Yes (0.88)	0.09	↓	↓	↑
α_{K_s}	–	Yes (0.89)	0.10	↑	–	–
C_{1K_s}	–	Yes (0.90)	0.07	–	↑	–
H_{K_s}	–	Yes (0.87)	0.13	–	–	–

*↑ means strong positive correlation, ↓ means strong negative correlation, and – means weak to medium correlation. m R_I^2 is the modified coefficient of determination for infiltration scaling.

A set of space–time rain fields was created from large-size steady rainfall fields, which were essentially steady rain fields with advection. Under these space–time rainfall processes and scaling K_s fields, infiltration fields exhibited some different behavior from the case of steady rainfall because of the added dynamics, but many other features were retained. There were more variations in the time series of the various infiltration properties such as the field average infiltration rate compared to the case of steady rain. The rain heterogeneity under the condition of dry soil and the rain singularity showed the strongest, negative influence on the field average infiltration. As in the case of steady rain, the heterogeneity of a space–time rain process had a strong and positive effect on the heterogeneity of the infiltration field and a dominant and negative effect on the singularity and the sparseness of the latter. Both the singularity and the sparseness of a K_s field were strongly proportional to their respective properties of the corresponding infiltration field. An interesting phenomenon was observed in the numerical experiments under space–time rain: The scaling parameters of infiltration fields from homogeneous and close-to-homogeneous rain fields usually varied with the rain field parameters in the opposite direction to those from non-homogeneous rain. The same behavior was observed in some experiments under steady rain. A major difference between the space–time rain and the steady rain was the clear and consistent pattern of temporal trends manifested in the infiltration parameters in the space–time rainfall cases. The directions of the trends are determined by rain heterogeneity. The singularity and the sparseness of the infiltration field decreased in time if the rain field was relatively homogeneous, and the trends reversed when the heterogeneity of the rain field was high. The heterogeneity of the infiltration field had a rising temporal trend under relatively homogeneous rain.

The singularity and the sparseness of infiltration fields usually had the same temporal trend while the heterogeneity of infiltration field changed in the opposite direction. These trends can be in time or in the variation with rain or K_s parameters. For instance, if an infiltration field subject to space–time rain becomes less singular in time, it most likely also becomes less sparse (or more space filling) and more heterogeneous, and vice versa. These findings reveal the internal connections among the scaling parameters of infiltration process.

The relationships between the scaling behaviors and the UM parameters of the driving fields and those of the resulting infiltration fields provide improved knowledge of the variables controlling the spatial infiltration patterns. Such insight can be useful for focusing on the dominant spatial processes in similar landscapes, where intense rainfall events drive Hortonian overland flow and infiltration processes. Scaling behavior of infiltration in such landscapes may also be inferred from the topography and surrogate measures of K_s across a watershed.

Acknowledgements

This work has been undertaken as part of the Specific Cooperative Agreement (SCA) between the USDA Agriculture Research Service and

Colorado State University. Funds provided by the SCA project 'Quantifying Space–Time Variability in Agricultural Landscapes' are appreciated.

Appendix A

The formulas for generating a conservative physical field, ε_λ, using UM model are (Pecknold et al., 1993)

$$\varepsilon_\lambda = e^{\Gamma_\lambda} \tag{A1}$$

$$\tilde{\Gamma}_\lambda = \Im^{-1}\left\{\left(\frac{C_1}{\alpha-1}\right)^{1/\alpha}\tilde{S}(\alpha)k^{-d/\alpha'}f(\lambda,\underline{k})\kappa_{\mathrm{d}}(\lambda)\right\} \tag{A2}$$

where λ is scale ratio; $\tilde{\Gamma}_\lambda$ is the Fourier transform of generator Γ_λ; $\Im^{-1}$ represents inverse Fourier transform; k is wavenumber vector and k is wavenumber vector modulus; $\tilde{S}$ is Lévy noise in Fourier space; d is the dimension of the underlying space; $\alpha' = \alpha/(\alpha-1)$; κ is a factor that makes up the difference between a continuous Fourier transform and the discrete fast Fourier transform (FFT); and the function $f(\lambda,\underline{k})$ is 1 for $k \leq \lambda$ and decaying exponentially for $k > \lambda$ to filter out wave numbers greater than λ.

A non-conservative field, V, is derived from its fluctuation, ΔV, which is generated using the following equation:

$$\Delta V_\lambda = \Im^{-1}\{\tilde{\varepsilon}_k k^{-H}\} \tag{A3}$$

where $\tilde{\varepsilon}$ is the Fourier transform of the underlying conservative field ε. The operation described by Eq. (A3) is a fractional integration of order H. Thus, a fractional differentiation of order H is required to derive the conservative field ε from the non-conservative field ΔV.

References

Ahuja, L., Naney, J.W., Green, R.E., Nielsen, D.R., 1984. Macroporosity to characterize spatial variability of hydraulic conductivity and effects of land management. Soil Sci. Soc. Am. J. 48, 699–702.

Bresler, E., Dagan, G., 1983. Unsaturated flow in spatially variable fields 2. Application of water flow models to various fields. Water Resour. Res. 19, 421–428.

Dagan, G., Bresler, E., 1983. Unsaturated flow in spatially variable fields 1. Derivative of models of infiltration and redistribution. Water Resour. Res. 19, 413–420.

Govindaraju, R.S., Morbidelli, R., Corradini, C., 2001. Areal infiltration modeling over soils with spatially correlated hydraulic conductivities. J. Hydrol. Eng. 6, 150–158.

Green, T.R., Erskine, R.H., 2004. Measurement, scaling, and topographic analyses of spatial crop yield and soil water content. Hydrol. Proc. 18, 1447–1465.

Green, W.H., Ampt, G.A., 1911. Studies on soil physics. J. Agric. Sci. 4, 1–24.

Gupta, V.K., Waymire, E.C., 1990. Multiscaling properties of spatial rainfall and river distributions. J. Geophys. Res. 95 (D3), 1999–2009.

Harris, D., Menabde, M., Seed, A., Austin, G., 1996. Multifractal characterization of rain fields with a strong orographic influence. J. Geophys. Res. 101, 26405–26414.

Lavallée, D., Lovejoy, S., Schertzer, D., Ladoy, P., 1993. Nonlinear variability of landscape topography: multifractal analysis and simulation. In: De Cola, L., Lam, N.S. (Eds.), Fractal in Geography, Prentice Hall, Englewood Cliffs, NJ, pp. 158–192.

Liu, H.H., Molz, F.J., 1997. Multifractal analyses of hydraulic conductivity distributions. Water Resour. Res. 33, 2483–2488.

Loague, K., Gander, G.A., 1990. R-5 revisited 1. Spatial variability of infiltration on a small rangeland catchment. Water Resour. Res. 26, 957–971.

Lovejoy, S., Schertzer, D., 1990. Multifractals, universality classes and satellite and radar measurements of cloud and rain fields. J. Geophys. Res. 95, 2021–2034.

Maller, R.A., Sharma, M.L., 1981. An analysis of areal infiltration considering spatial variability. J. Hydrol. 52, 25–37.

Meng, H., 2004. Multifractal analysis of the effects of rainfall and K_s on surface infiltration and runoff, PhD Dissertation, Colorado State University, Fort Collins, Colorado, USA.

Nash, J.E., Sutcliffe, J.V., 1970. River flow forecasting through conceptual models. 1. A discussion of principles. J. Hydrol. 10, 282–290.

Olsson, J.M., Persson, J., Albergel, J., Berndtsson, R., Zante, P., Oehrstroem, P., Nasri, S., 2002. Multiscaling analysis and random cascade modeling of dye infiltration. Water Resour. Res. 38.

Over, T.M., Gupta, V.K., 1994. Statistical analysis of mesoscale rainfall: dependence of a random cascade generator on large-scale forcing. J. Appl. Meteorol. 33, 1526–1542.

Parisi, G., Frisch, U., 1985. A multifractal model of intermittency. In: Ghil, M., Benzi, R., Parisi, G. (Eds.), Turbulence and Predictability in Geophysical Fluid Dynamics and Climate Dynamics. North-Holland, Amsterdam, pp. 84–88.

Pecknold, S., Lovejoy, S., Schertzer, D., Hooge, C., Malouin, J.F., 1993. The simulation of universal multifractals. In: Perdand, J.M., Lejeune, A. (Eds.), Cellular Automata: Prospects in Astrophysical Applications, World Scientific, Singapore, pp. 228–267.

Peters-Lidard, C.D., Pan, F., Wood, E.F., 2001. A re-examination of modeled and measured soil moisture spatial variability and its implications for land surface modeling. Adv. Water Resour. 24, 1069–1083.

Revol, P., Clothier, B.E., Vauclin, M., 1997. Infiltration from a surface point source and drip irrigation. 2. An approximate time-dependent solution for wet-front position. Water Resour. Res. 33.

Rodriguez-Iturbe, I., Vogel, G.K., Rigon, R., Entekhabi, D., Castelli, F., Rinaldo, A., 1995. On the spatial organization of soil moisture fields. Geophys. Res. Lett. 22, 2757–2760.

Schertzer, D., Lovejoy, S., 1987. Physical modeling and analysis of rain and clouds by anisotropic, scaling multiplicative processes. J. Geophys. Res. 92, 9693–9714.

Schmitt, F., Lovejoy, F.S., Schertzer, D., 1995. Multifractal analysis of the Greenland ice-core project climate data. Geophys. Res. Lett. 22, 1689–1692.

Sivapalan, M., Wood, E.F., 1986. Spatial heterogeneity and scale in the infiltration response of catchments. In: Gupta, V.K., Rodriguez-Iturbe, I., Wood, E.F. (Eds.), Scale Problems in Hydrology. Reidel Publishing Company, Dordrecht, pp. 81–106.

Tarboton, D.G., 1997. A new method for the determination of flow directions and upslope areas in grid digital elevation models. Water Resour. Res. 33, 309–319.

Tennekoon, L., Boufadel, M.C., Lavallee, D., Weaver, J., 2003. Multifractal anisotropic scaling of the hydraulic conductivity. Water Resour. Res. 39, 1193.

Tessier, Y., Lovejoy, S., Schertzer, D., 1993. Universal multifractals: theory and observations for rain and clouds. J. Appl. Meteorol. 32, 223–250.

Tessier, Y., Lovejoy, S., Hubert, P., Schertzer, D., Pecknold, S., 1996. Multifractal analysis and modeling of rainfall and river flows and scaling, causal transfer functions. J. Geophys. Res. 101, 26427–26440.